Available online at www.sciencedirect.com
ScienceDirect
International Journal of Heat and Mass Transfer 51 (2008) 1293–1312
International Journal of HEAT and MASS TRANSFER
www.elsevier.com/locate/ijhmt

Assessment by comparison with DNS data of turbulence models used in simulations of mixed convection

W.S. Kim [a], S. He [a,*], J.D. Jackson [b]

[a] School of Engineering, University of Aberdeen, Aberdeen AB24 3UE, UK
[b] Simon Building, University of Manchester, Manchester M13 9PL, UK

Received 2 February 2007; received in revised form 26 November 2007
Available online 31 January 2008

Abstract

The paper presents an assessment of the performance of a variety of turbulence models in simulating buoyancy-aided, turbulent mixed convection in vertical pipes. This has been done by comparison of RANS predictions with DNS results already available in the literature. Both the RANS and the DNS studies were conducted for conditions of constant and uniform fluid properties with the influence of buoyancy being accounted for using the Boussinesq approximation. This eliminated effects of non-uniformity of properties other than through the action of buoyancy and enabled its influence to be considered in isolation. In the course of the study, the turbulence models have been classified into two groups, namely, those which were able to capture the main features of buoyancy-influenced heat transfer (Group one) and those that were not able to do so (Group two). Common features in model formulation have been identified for each group. It is shown that the response to buoyancy of commonly-used controlling parameters in turbulence damping functions varies significantly and that the performance of a model can largely be correlated with the type of controlling parameter used. A significant defect of the Group-one models which has been identified is that they continue to predict that the 'viscous sub-layer' remains thick as a result of the influence of buoyancy even when the velocity profile has been distorted to an extent that it has become inverted in the core, whereas DNS data clearly show that this is not the case. The use of different methodologies for modelling direct production of turbulence through the direct action of buoyancy has been shown to have little effect on predictions of mixed convection in vertical flows because the effect of buoyancy on turbulence is predominantly due to the indirect effect.

Keywords: Mixed convection; Buoyancy; Turbulence models; Variable properties

1. Introduction

1.1. General background

Turbulent mixed convection in vertical channels is an important mode of heat transfer that can be found in heat exchangers, nuclear reactors, chemical plant, cooling systems for electronic components, and many other items of industrial plant. Despite the relatively simple geometry involved in many of these applications, the flow and heat transfer can be extremely difficult to predict, especially when the influences of buoyancy are coupled with non-uniformity of thermal properties. The effects of buoyancy can either enhance the heat transfer process or impair it depending on the flow rate, the thermal loading, and the flow direction. The behaviour is quite different for laminar and turbulent mixed convection.

In the case of laminar mixed convection in a vertical passage, heat transfer is impaired in buoyancy-opposed flow and enhanced in buoyancy-aided flow. These effects are a consequence of the distortion of the velocity field and the effect that this has on the balance between diffusion and advection. With downward flow in a heated pipe, buoyancy opposes the flow and the velocity of the fluid in the vicinity of the heated surface is reduced, energy transport by advection is reduced and the effectiveness of heat transfer is impaired relative to that for laminar forced

* Corresponding author. Tel.: +44 1224 272799; fax: +44 1224 272497.
E-mail address: s.he@abdn.ac.uk (S. He).

0017-9310/$ - see front matter © 2007 Elsevier Ltd. All rights reserved.
doi:10.1016/j.ijheatmasstransfer.2007.12.002

Nomenclature

Bo^*	buoyancy parameter, $[=Gr^*/(Re^{3.425}Pr^{0.8})]$
$C_{\varepsilon 1}$, $C_{\varepsilon 2}$	constants in the ε-equation
C_μ	constant in constitutive equation of eddy viscosity model
D	additional term in the k-equation
E	additional term in the ε-equation
E_k	dissipation term
f	elliptic relation parameter
f_1, f_2	functions in dissipation equation
f_μ	damping function in the constitutive equation
g	acceleration due to gravity
G_k	buoyant production
Gr^*	Grashof number, $Gr^* = \beta g D^4 q_w/(\lambda \upsilon^2)$
h	heat transfer coefficient, $q_w/(T_w - T_b)$; enthalpy
k	turbulent kinetic energy
Nu	Nusselt number, $Nu = hD/\lambda$
Nu_f	Nusselt number for forced convection
p	pressure
P_k	turbulent shear production
Pr	Prandtl number, $Pr = \mu c_p/\lambda$
Pr_t	turbulent Prandtl number
q_w	convective heat flux from the wall
Re	Reynolds number, $Re = u_b D/\upsilon$
T_b	bulk temperature
T_w	wall temperature
$\overline{t^2}$	temperature variance
U_b	bulk velocity
U, V	velocity components in z, r-directions
$\overline{uv}$	turbulent shear stress
$\overline{v^2}$	variance of the normal component of turbulent velocity
x	axial distance from start of heating
y	distance from pipe wall in the direction normal to it
y^+	non-dimensional distance from pipe wall, $y(\tau_w/\rho)^{1/2}/\upsilon$

Greek symbols

ε	modified dissipation rate of k
ε'	dissipation rate of k
ε^2	dissipation rate of $\overline{t^2}$
λ	thermal conductivity
μ	molecular viscosity
μ_t	turbulent viscosity
υ	kinematic viscosity, $\upsilon = \mu/\rho$
ρ	density
σ_k, σ_ε	turbulent Prandtl number for k and ε

Subscripts

b	bulk
cp	constant property
f	forced
w	wall

convection. With upward flow in a heated pipe, buoyancy aids the flow, the velocity near the heated surface is increased, energy transport by advection is increased and the effectiveness of heat transfer is improved in relation to that for forced convection.

The situation is very different in the case of turbulent mixed convection. Although the effect of buoyancy opposing the flow in the near wall region is still to reduce advection, a further consequence is that the shear stress in that region is increased. As a result, turbulence production is enhanced (see Fig. 1) and the turbulent diffusion of heat is improved. In practice, the second of these two effects dominates with the result that the effectiveness of heat transfer improves. In the buoyancy-aided case, although the advection in the near-wall region is increased, the shear stress in that region is reduced (see Fig. 1), turbulence production is reduced, and the turbulent diffusion of heat is impaired. The net result is that heat transfer is less effective. As the buoyancy influence is progressively increased, the impairment of turbulence production and the deterioration of heat transfer become more and more marked. A stage is reached where the shear stress in the near-wall falls to such a level that, the flow is effectively laminarized (again see Fig. 1). With further increase of buoyancy influence, the shear stress in the core region becomes negative and turbulence starts to be produced in that region. The effectiveness of heat transfer then recovers.

These interesting effects of buoyancy on turbulent flow and heat transfer were explained by Jackson and Hall [1]. Based on simple arguments, they developed a semi-empirical model for fully developed turbulent mixed convection heat transfer in a uniformly heated vertical passage. By relating the modified stress in the near-wall region to heat transfer using empirical equations for friction and forced convection in pipe flow, the following semi-empirical equation was obtained:

$$\frac{Nu}{Nu_f} = \left(\left| 1 \pm 2.5 \times 10^5 Bo^* \left(\frac{Nu}{Nu_f} \right)^{-2} \right| \right)^{0.46} \quad (1)$$

In the above equation, the plus and minus signs apply to the buoyancy-opposed and buoyancy-aided cases, respectively, Nu is the Nusselt number for mixed convection, Nu_f is the Nusselt number for conditions of negligible buoyancy influence (forced convection) and Bo^* is a parameter which combines Grashof number Gr^*, Reynolds number Re and Prandtl number Pr in the form $Gr^*/(Re^{3.425}Pr^{0.8})$ to characterise the strength of buoyancy influences.

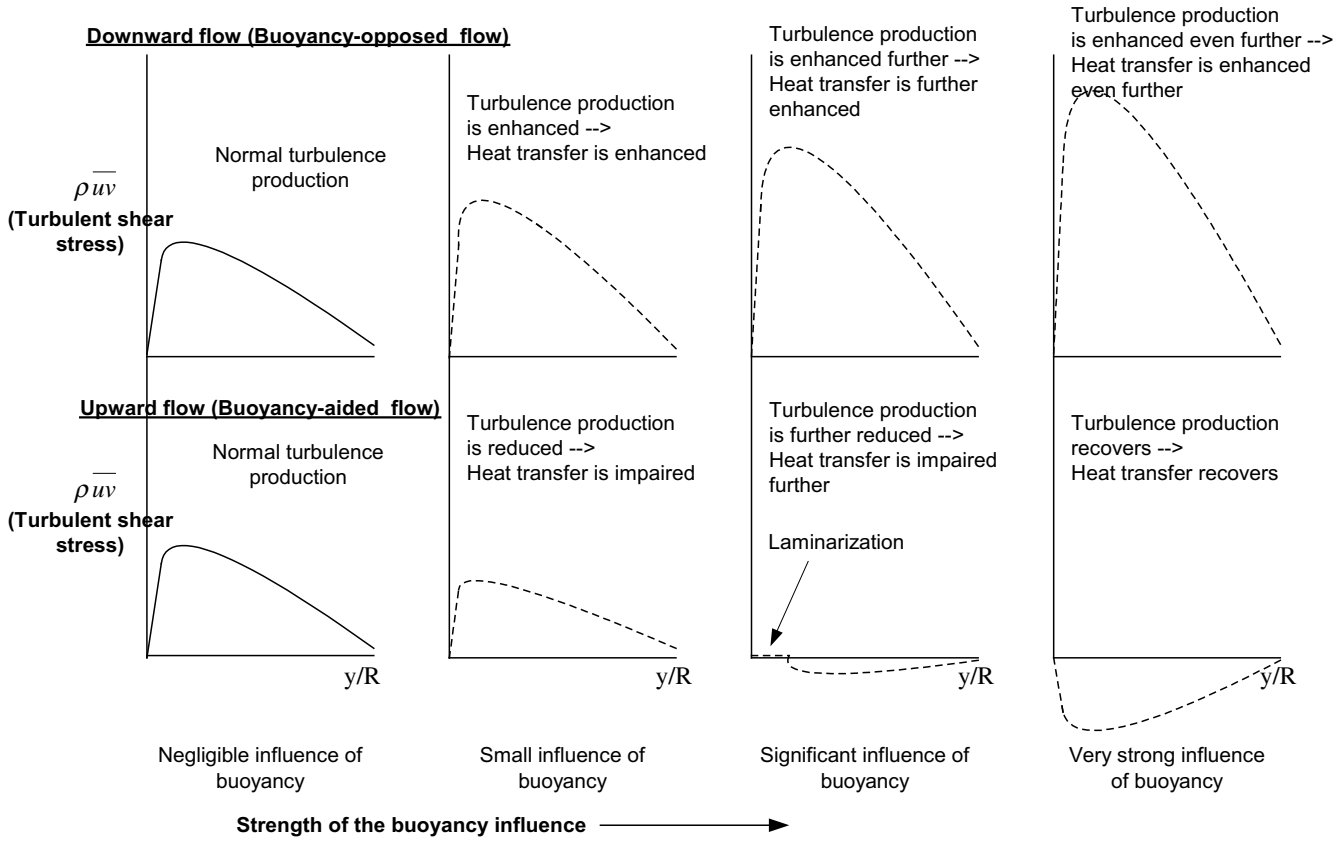

Fig. 1. Turbulent shear stress for buoyancy-opposed and buoyancy-aided flow.

1.2. Overview of earlier studies of turbulent mixed convection

Mixed convection in vertical passages has been studied extensively over the past 60 years or so. A detailed review of the work in the period up to the end of the nineteen eighties can be found in Jackson et al. [2] and an updated review can be found in a recent paper by Jackson [3]. In this section, only a brief review of relevant work is given and attention is restricted to the buoyancy-aided case.

1.2.1. Experimental studies

The experiments with buoyancy-aided (upward) flow of Byrne and Ejiogu [4] in the early 1970s showed impairment of the effectiveness of heat transfer with onset of buoyancy influence followed by recovery. However, they were limited by the fact that the length to diameter ratio of the test section was quite small which limited the scope of that study. Around the same time, Steiner [5], using a much longer test section (length to diameter ratio about 60), measured radial profiles of velocity and temperature at various axial locations and also distributions of heat transfer coefficient. These indicated that buoyancy influences tend to reduce turbulence and impair heat transfer. Such effects developed rather gradually. Later, Carr et al. [6] measured radial profiles of velocity and temperature at the downstream end of a very long heated tube and found that as the velocity profile became appreciably distorted by buoyancy influences, turbulence was reduced and the effectiveness of heat transfer was impaired. More recently, Polyakov and Shindin [7] made measurements of heat transfer and also of velocity and turbulence in a long tube and found that turbulent heat transfer near the wall was suppressed to a greater degree than momentum transport by the influence of buoyancy. Under conditions of very strong buoyancy influence, turbulence was suppressed near the wall but readily generated in the core region. The more recent experiments include those of Vilemas et al. [8] and Li and Jackson [9], who also made detailed measurements of local heat transfer in very long uniformly heated tubes. Heat transfer regimes with both monotonic and non-monotonic distributions of wall temperature were found. Under conditions where heat transfer was impaired, the thermal development was very slow and a fully developed condition was only approached at axial locations well downstream, about 100 diameters after the start of heating.

1.2.2. Computational studies

Attempts have been made to simulate buoyancy-influenced turbulent convective heat transfer in vertical tubes using a variety of computational formulations and turbulence models. In an early study, Tanaka et al. [10] used a modification of the Reichardt eddy diffusivity model. This approach did not prove to be suitable for buoyancy-influenced flow because the turbulent viscosity was prescribed

as a function of distance from the surface without any reference to local features of the flow. Walklate [11] used both mixing length models and k–ε models to simulate the experiments of Carr et al. [6]. He found that the low-Reynolds number k–ε models performed better than both the standard k–ε model and the mixing length models.

More recently, the understanding of turbulent mixed convection has been aided considerably by the work of Cotton [12]. He used the low-Reynolds number k–ε turbulence model of Launder–Sharma [13], in a parabolic developing wall shear flow computational formulation with constant properties with the influence of buoyancy accounted for using the Boussinesq approximation. The code was used with considerable success for simulating some of the earlier experiments on buoyancy-aided mixed convection in vertical tubes – see [14]. They reported simulations of the experiments due to Carr et al. [6] and Steiner [5] and generally found acceptable agreement with the experimental data. Later, Mikielewicz [15] carried out a comparative study of the performance of a number of turbulence models. That study was largely limited to comparisons of predictions of effectiveness of heat transfer with experimental data. The models of Launder–Sharma [13] and Chien [16] were found to generally perform better than the rest. A study of upward mixed convection of air flow in a long vertical tube has been conducted by Behzadmehr et al. [17] for two rather low-Reynolds numbers ($Re = 1000$ and 1500) over a range of Grashof numbers ($Gr \leqslant 10^8$) using the Launder–Sharma model. The fluid properties were assumed constant except for the density in the body force term. They identified two critical Grashof numbers for each Reynolds number, which correspond to laminar–turbulent transition and relaminarization of the flow.

Recently direct numerical simulation (DNS) has been used in studies of mixed convection in vertical channels. Kasagi and Nishimura [18] conducted one of the earliest studies of this kind. The initial Reynolds number was fixed at 4300 but several values of Grashof number was used. The simulations provided much more detailed information on turbulence than could be obtained from experiments. The results clearly showed that buoyancy modifies the force balance which governs the distribution of the Reynolds shear stress and the shear production rate of turbulent kinetic energy, causing heat transfer enhancement or impairment. More recently You et al. [19] conducted a DNS study on turbulent mixed convection in a heated vertical tube for conditions where the fluid properties were assumed to be uniform and buoyancy was accounted for using the Boussinesq approximation. This work has been followed by a DNS study of mixed convection heat transfer to carbon dioxide at supercritical pressure [20], where the effects of the very significant non-uniformity of fluid properties have been fully accounted for.

1.3. The present study

In contrast to the vast amount of heat transfer data available for mixed convection in vertical channels, detailed measurements of velocity and turbulence are rather limited. Information on the near-wall behaviour of turbulence is particularly difficult to obtain and such data are therefore very sparse. This to some extent has limited the assessments which have been made of the performance of turbulence models for conditions of mixed convection and hampered progress in improving the capability of turbulence models to predict such flows.

The development of DNS has changed the situation and detailed data on velocity and turbulence are now becoming available. The objective of the present study is to take advantage of this and to conduct a detailed and systematic assessment of the performance of a range of turbulence models against DNS data. It is hoped that this will lead to an improved understanding of the underlying reasons for the observed performance of the various turbulence models and shed some light on improvements which might be made to them. For this purpose, the DNS data due to You et al. [19] has been selected for use. An attractive feature of these data, which is impossible to achieve experimentally, is that the simulations were conducted with uniform fluid properties but using the Bousinesq approximation to account for the influence of buoyancy. This has enabled its effect to be studied in isolation from effects of non-uniformity of fluid properties.

The DNS studies considered here were conducted for conditions of fully developed turbulent mixed convection heat transfer to air ($Pr = 0.71$) flowing in a vertical pipe at a Reynolds number of 5300. Both buoyancy-aided and -opposed flows were considered. However, in this study, we have focused on the buoyancy-aided cases since they are often of particular importance in engineering applications and the physical processes involved are especially interesting and challenging to understand and to predict. Three DNS mixed convection cases have been considered.

Table 1
A summary of conditions in the simulations

RANS simulations											
Case	Forced	(1)	(2) or (a)	(3) or (b)	(4)	(5)	(6)	(7) or (c)	(8)	(9)	(10)
Bo^* ($\times 10^6$)	0.0	1.0	1.6	2.3	3.0	4.0	5.0	6.3	8.0	10.0	30.0
DNS											
Case	Forced		(a)	(b)				(c)			
Bo^* ($\times 10^6$)	0.0		1.6	2.3				6.3			

These have values of buoyancy parameter Bo^* of 1.6×10^{-6}, 2.3×10^{-6}, and 6.3×10^{-6} (referred to as Cases a, b, and c). A forced convection case ($Bo^*=0$) was also computed for comparison. In order to establish the trends with increasing buoyancy influence, additional simulations covering an extended range of buoyancy parameter have also been carried out. A summary of the conditions covered is given in Table 1.

2. Numerical method

The elliptic computational formulation used in this study solved the governing equations for two-dimensional developing flow and convective heat transfer using Reynolds-averaged conservation equations. As in the DNS work, thermal properties are taken to be constant and the effect of buoyancy in the momentum equation is accounted for using the Boussinesq approximation. We are particularly concerned with 'low-Reynolds number' eddy viscosity turbulence models since that feature has been found in earlier studies to be essential to simulate 'non-equilibrium' flows such as these under consideration here. We aim to cover a spectrum of such models but with main emphasis on those which were targeted at improving mixed convection heat transfer. With this in mind we have selected some '*classical*' k–ε models: Launder–Sharma (LS) [13], Lam–Bremhorst (LB) [21], Chien (CH) [16], a k–ω model, Wilcox (WI) [22] and some more recent models: Myoung–Kasagi (MK) [23], Yang–Shih (YS) [24], Abe–Kondoh–Nagano (AKN) [25], Cotton–Kirwin (CK) [26], and Hwang–Lin (HL) [27]. The k–ε–v^2–f model of Durbin (V2F) [28] has also been included since, in some recent studies of variable property heat transfer [29,30], this model has been found to perform better than many k–ε models. In addition, a four-equation k–ε–t^2–ε_t model due to Abe, Kondoh and Nagano [31] has also been included. This incorporates a turbulent heat transfer model into a basic k–ε flow model which enables the time scale for the thermal field to be decoupled from that for the momentum and therefore allows the turbulent Prandtl number to be modelled rather than specified.

The governing equations for the mean flow and energy transport written in cylindrical coordinates are as follows:

Continuity

$$\frac{1}{r}\left\{\frac{\partial}{\partial x}(rU)+\frac{\partial}{\partial r}(rV)\right\}=0 \tag{2}$$

U-momentum

$$\frac{1}{r}\left\{\frac{\partial}{\partial x}(rU^2)+\frac{\partial}{\partial r}(rVU)\right\}=-\frac{1}{\rho}\frac{\partial p}{\partial x}+g\beta(T-T_{\mathrm{ref}})+\frac{1}{r}\left\{2\frac{\partial}{\partial x}\left[rv_{\mathrm{e}}\left(\frac{\partial U}{\partial x}\right)\right]+\frac{\partial}{\partial r}\left[rv_{\mathrm{e}}\left(\frac{\partial U}{\partial r}+\frac{\partial V}{\partial x}\right)\right]\right\} \tag{3}$$

V-momentum

$$\frac{1}{r}\left\{\frac{\partial}{\partial x}(rUV)+\frac{\partial}{\partial r}(rV^2)\right\}=-\frac{1}{\rho}\frac{\partial p}{\partial r}+\frac{1}{r}\left\{\frac{\partial}{\partial x}\left[rv_{\mathrm{e}}\left(\frac{\partial V}{\partial x}+\frac{\partial U}{\partial r}\right)\right]+2\frac{\partial}{\partial r}\left[rv_{\mathrm{e}}\left(\frac{\partial V}{\partial r}\right)\right]\right\}-2\frac{v_{\mathrm{e}}V}{r^2} \tag{4}$$

where v_{e} is the effective viscosity defined by $v_{\mathrm{e}}=v+v_{\mathrm{t}}$, and v_{t} is the turbulent viscosity.

Energy

$$\frac{1}{r}\left\{\frac{\partial}{\partial x}(rUh)+\frac{\partial}{\partial r}(rVh)\right\}=\frac{1}{r}\left\{\frac{\partial}{\partial x}\left[r\left(\frac{v}{Pr}+\frac{v_{\mathrm{t}}}{Pr_{\mathrm{t}}}\right)\frac{\partial h}{\partial x}\right]+\frac{\partial}{\partial r}\left[r\left(\frac{v}{Pr}+\frac{v_{\mathrm{t}}}{Pr_{\mathrm{t}}}\right)\frac{\partial h}{\partial r}\right]\right\} \tag{5}$$

where Pr is the molecular Prandtl number and Pr_t is the turbulent Prandtl number.

The constitutive equation and the transport equations for k and ε are as follows:

Constitutive equation

$$v_{\mathrm{t}}=C_\mu f_\mu\frac{k^2}{\varepsilon} \tag{6}$$

where f_μ is a damping function to account for near-wall effects and C_μ is a constant.

Turbulent kinetic energy

$$\left[\frac{\partial(Uk)}{\partial x}+\frac{1}{r}\frac{\partial(rVk)}{\partial r}\right]=\frac{\partial}{\partial x}\left[\left(v+\frac{v_{\mathrm{t}}}{\sigma_k}\right)\frac{\partial k}{\partial x}\right]+\frac{1}{r}\frac{\partial}{\partial r}\left[r\left(v+\frac{v_{\mathrm{t}}}{\sigma_k}\right)\frac{\partial k}{\partial r}\right]+P_k+G_k-(\varepsilon-D) \tag{7}$$

in which ε ($=\varepsilon'+D$) is the modified dissipation of k, ε' the originally-defined dissipation of k, and D a damping function. For some turbulence models, $D=0$, and for those models $\varepsilon=\varepsilon'$. Other terms in Eq. (7) are defined as

$$P_k=v_{\mathrm{t}}\left[2\left\{\left(\frac{\partial U}{\partial x}\right)^2+\left(\frac{\partial V}{\partial r}\right)^2+\left(\frac{V}{r}\right)^2\right\}+\left(\frac{\partial U}{\partial r}+\frac{\partial V}{\partial x}\right)^2\right]$$

(shear production)

and G_k is gravitational production which is modelled using the GGDH approximation, detailed in the Appendix, in most simulations. Effect of using alternative models was studied (see Section 4.3.4).

Dissipation rate of turbulent kinetic energy

$$\left[\frac{\partial(U\varepsilon)}{\partial x}+\frac{1}{r}\frac{\partial(rV\varepsilon)}{\partial r}\right]=\frac{\partial}{\partial x}\left[\left(v+\frac{v_{\mathrm{t}}}{\sigma_\varepsilon}\right)\frac{\partial\varepsilon}{\partial x}\right]+\frac{1}{r}\frac{\partial}{\partial r}\left[r\left(v+\frac{v_{\mathrm{t}}}{\sigma_\varepsilon}\right)\frac{\partial\varepsilon}{\partial r}\right]+C_{\varepsilon1}f_1\frac{1}{T}P_k+C_{\varepsilon1}f_1\frac{1}{T}G_k-C_{\varepsilon2}f_2\frac{\varepsilon}{T}+E, \tag{8}$$

where $T=k/\varepsilon$.

The V2F model has two additional equations (for $\overline{v^2}$ and f) and additional parameters as shown below [28].

Turbulent velocity scale ($\overline{v^2}$)

$$\left[\frac{\partial(U\overline{v^2})}{\partial x}+\frac{1}{r}\frac{\partial(rV\overline{v^2})}{\partial r}\right]=\frac{\partial}{\partial x}\left[\left(\nu+\frac{\nu_t}{\sigma_k}\right)\frac{\partial\overline{v^2}}{\partial x}\right]+\frac{1}{r}\frac{\partial}{\partial r}\left[r\left(\nu+\frac{\nu_t}{\sigma_k}\right)\frac{\partial\overline{v^2}}{\partial r}\right]+kf-6\overline{v^2}\frac{\varepsilon}{k} \tag{9}$$

Production (f)

$$0=\frac{\partial}{\partial x}\left(\frac{\partial f}{\partial x}\right)+\frac{1}{r}\frac{\partial}{\partial r}\left(r\frac{\partial f}{\partial r}\right)-\frac{1}{L^2}f+\frac{(C_1-1)}{L^2}\times\frac{(2/3-\overline{v^2}/k)}{T}+\frac{C_2}{L^2}\frac{1}{\rho k}(P_k)+\frac{1}{L^2}\frac{5\overline{v^2}/k}{T} \tag{10}$$

where

$$\nu_t=C_\mu\overline{v^2}T,\quad \text{where}\quad T=\max\left[\frac{k}{\varepsilon},6\sqrt{\frac{\nu}{\varepsilon}}\right],$$

$$L=C_L\max\left[\frac{k^{3/2}}{\varepsilon},C_\eta\left(\frac{\nu^3}{\varepsilon}\right)^{1/4}\right]$$

$$C_1=1.4,\quad C_2=0.3,\quad C_\eta=70,\quad C_\mu=0.22,\quad C_L=0.23$$

The model constants and functions are listed in Table 2.

In the present study, the computational domain, which consists of an unheated section followed by an extremely long heated one (over 480 diameters), was discretized into a mesh of grids, typically, 120 × 106 (axial × radial). The relative sparseness of the mesh in the axial direction does not introduce a problem as only fully developed results near the pipe exit are of interest in this study. The mesh was carefully adjusted radially in each individual run to ensure that the near-wall flow features were properly resolved. This included ensuring that the y^+ value at the first node of the mesh was less than 0.5. The QUICK scheme was used for approximating the convection terms in the momentum equations, and the SMART scheme was used for other transport equations to improve numerical stability. The SIMPLE scheme was used for coupling the pressure and the velocity fields. The resulting five-point coefficient matrix system was solved iteratively using the line-by-line TDMA algorithm. That is, variables at a particular line were solved simultaneously and these at the neighbouring lines were assumed to be known, values from the previous iteration being used.

3. Forced convective heat transfer with constant uniform properties

To obtain an initial assessment of the performance of the turbulence models which are being examined in this study, calculations were first made for conditions of forced convection, i.e., with buoyancy absent and uniform fluid properties. Values of friction coefficient and Nusselt number obtained using the various turbulence models are shown in Fig. 2 along with the DNS results and values calculated using the empirical equations shown below for friction and heat transfer, respectively.

$$C_f=0.079Re^{-0.25}\quad\text{(Blasius)} \tag{11}$$

$$Nu_f=\frac{RePr\left(\frac{f}{8}\right)}{1.07+\frac{900}{Re}-\frac{0.63}{1+10Pr}+12.7\sqrt{\frac{f}{8}}\left(Pr^{\frac{2}{3}}-1\right)}\quad[32] \tag{12}$$

It can be seen that the performance of the turbulence models is rather variable. The predicted values of Nusselt number range from about 17 (YS model) to about 21.5 (HL model) with the majority being higher than the DNS value of 18.2. The CH model value of about 18.7 is closest to the DNS value. The V2F, LS, and CK models also give values of Nusselt number which are in good agreement with the DNS results. Clearly the models have some limitations, even in terms of the extent to which they are able to describe fully developed heat transfer in a uniformly heated circular tube without any influences of the non-uniformity of fluid properties or buoyancy. The values of friction coefficient range from 0.0082 (YS model) to 0.0115 (HL model) being fairly evenly spread below and above the DNS. Those of the LS and AKN models lie 8% below and 6% above the DNS data respectively. There is a close correlation between the variation of c_f and Nu from model to model.

In the next section, the values of Nusselt number and friction coefficient for mixed convection obtained with each turbulence model will be normalized using the corresponding forced convection values obtained using that model. To some extent, this should reduce the importance of the variation in performance of the model for forced convection in this comparative study and therefore enable the assessment to be focused on the ability of the models to respond to the influence of buoyancy.

4. Turbulent mixed convection

4.1. Nusselt number and friction coefficient

4.1.1. Nusselt number

Fig. 3 shows the ratio of the Nusselt number in mixed convection and that for forced convection at corresponding conditions versus the buoyancy parameter for the three DNS mixed convection cases and for the simulations of those cases using the various turbulence models. Also shown in the figure are the values for the additional simulations covering an extended range of buoyancy parameter in order to establish the trend of the variations.

As explained in Section 1, although heat transfer in a buoyancy-aided flow is influenced by both the modification of the mean flow field and the reduction/enhancement of turbulence, the latter effect is dominant in most cases. As a result buoyancy-aided flows are most readily categorised in terms of the effect of buoyancy on the turbulence: (a) a

Table 2
Details of the turbulence models

Model	Code	C_μ	$C_{\varepsilon 1}$	$C_{\varepsilon 2}$	σ_k	σ_ε
(*a*) *Constants in the turbulence models*						
(1) Launder–Sharma (1974)	LS	0.09	1.44	1.92	1.0	1.3
(2) Chien (1982)	CH	0.09	1.35	1.80	1.0	1.3
(3) Lam–Bremhorst (1981)	LB	0.09	1.44	1.92	1.0	1.3
(4) Abe–Kondoh–Nagano (1994)	AKN	0.09	1.50	1.90	1.4	1.4
(5) Wilcox (1988)[a]	WI	0.09	1.55	1.83	2.0	2.0
(6) Yang–Shih (1993)	YS	0.09	1.44	1.92	1.0	1.3
(7) Myoung–Kasagi (1990)	MK	0.09	1.40	1.80	1.4	1.3
(8) Hwang–Lin (1998)	HL	0.09	1.44	1.92	[b]	[c]
(9) V2–F (1998)	V2F	0.22	1.4	1.9	1.0	1.3
(10) Cotton–Kirwin (1995)	CK	0.09	1.44	1.92	1.0	1.3,

Code	f_μ	f_1	f_2
(*b*) *Functions in the turbulence models*			
LS	$\exp\left[\frac{-3.4}{(1+Re_t/50)^2}\right]$	1.0	$1-0.3\exp(-Re_t^2)$
CH	$1-\exp(-0.0115y^+)$	1.0	$1-0.22\exp\left(\frac{-Re_t^2}{36}\right)$
LB	$[1-\exp(-0.0165Re_y)]^2\left(1+\frac{20.5}{Re_t}\right)$	$1+\left(\frac{0.05}{f_\mu}\right)^3$	$1-\exp(-Re_t^2)$
AKN	$\left[1+\frac{5}{Re_t^{0.75}}\exp\left(-\left(\frac{Re_t}{200}\right)^2\right)\right]\left(1-\exp\left(-\frac{y^*}{14}\right)\right)^2$	1.0	$\left\{1-0.3\exp\left(-\left(\frac{Re_t}{6.5}\right)^2\right)\right\}\left[1-\exp\left(-\frac{y^*}{3.1}\right)\right]^2$
WI	1.0	1.0	1.0
YS	$\left(1+1/\sqrt{Re_t}\right)\left[1-\exp\begin{pmatrix}-1.5\times10^{-4}Re_y\\-5.0\times10^{-7}Re_y^3\\-1.0\times10^{-10}Re_y^5\end{pmatrix}\right]^{0.5}$	$\frac{\sqrt{Re_t}}{1+\sqrt{Re_t}}$	$\frac{\sqrt{Re_t}}{1+\sqrt{Re_t}}$
MK	$[1-\exp(-y^+/70)]\left(1+\frac{3.45}{Re_t^{1/2}}\right)$	1.0	$\left\{1-\frac{2}{9}\exp\left(-\left(\frac{Re_t}{6}\right)^2\right)\right\}\left[1-\exp\left(-\frac{y^+}{5}\right)\right]^2$
HL	$1-\exp\left[-\frac{y_\lambda}{100}-\frac{8y_\lambda^3}{1000}\right]$	1.0	1.0
V2F	$\frac{\overline{v^2}}{k}$	$1+0.045\sqrt{\frac{k}{v^2}}$	1.0
CK	$1-0.97\exp\left(-\frac{Re_t}{160}\right)-0.0045Re_t\exp\left[-\left(\frac{Re_t}{200}\right)^3\right]$	1.0	1.0

Code	D	E	Wall BC
(*c*) *D and E terms and wall boundary conditions for k and ε*			
LS	$2\nu\left(\frac{\partial\sqrt{k}}{\partial y}+\frac{\partial\sqrt{k}}{\partial x}\right)^2$	$2\nu\nu_t\left[\left(\frac{\partial^2 V}{\partial x^2}\right)^2+\left(\frac{\partial^2 U}{\partial y^2}\right)^2\right]$	$k_w=0,\tilde{\varepsilon}_w=0$
CH	$2\nu k\left(\frac{1}{y^2}\right)$	$\frac{-2\nu\tilde{\varepsilon}}{y^2}\exp(-0.5y^+)$	$k_w=0,\tilde{\varepsilon}_w=0$
LB	0	0	$k_w=0,\varepsilon_w=\nu\frac{\partial^2 k}{\partial y^2}$
AKN	0	0	$k_w=0,\varepsilon_w=2\nu\frac{k}{y^2}$
WI[c]	0	$-2\left(\nu+\frac{\nu_t}{2}\right)\left(\frac{\partial k}{\partial y}+\frac{\partial k}{\partial x}\right)\left[\frac{\partial}{\partial y}\left(\frac{\varepsilon}{k}\right)+\frac{\partial}{\partial x}\left(\frac{\varepsilon}{k}\right)\right]$	$k_w=0,\varepsilon_w=\nu\frac{\partial^2 k}{\partial y^2}$
YS	0	$2\nu\nu_t\left[\left(\frac{\partial^2 V}{\partial x^2}\right)^2+\left(\frac{\partial^2 U}{\partial y^2}\right)^2\right]$	$k_w=0,\varepsilon_w=2\nu\left(\frac{\partial\sqrt{k}}{\partial y}\right)^2$
MK	0	0	$k_w=0,\varepsilon_w=\nu\frac{\partial^2 k}{\partial y^2}$
HL	$2\nu\left(\frac{\partial\sqrt{k}}{\partial y}+\frac{\partial\sqrt{k}}{\partial x}\right)^2-\frac{1}{2}\nu\frac{\partial}{\partial y}\left(\frac{k}{\tilde{\varepsilon}}\frac{\partial\tilde{\varepsilon}}{\partial y}\right)$	$-\nu\frac{\partial}{\partial y}\left(\frac{\tilde{\varepsilon}}{k}\frac{\partial k}{\partial y}\right)$	$k_w=0,\tilde{\varepsilon}_w=0$
V2F	0	0	$k_w=0,\varepsilon_w=\nu\frac{\partial^2 k}{\partial y^2}$
CK	$2\nu\left(\frac{\partial\sqrt{k}}{\partial y}+\frac{\partial\sqrt{k}}{\partial x}\right)^2$	$0.95\nu\nu_t\left[\left(\frac{\partial^2 V}{\partial x^2}\right)^2+\left(\frac{\partial^2 U}{\partial y^2}\right)^2\right]$	$k_w=0,\tilde{\varepsilon}_w=0$
Note	$Re_t=\frac{k^2}{\nu\varepsilon}$, $Re_y=\frac{y k^{1/2}}{\nu}$, $y^+=\frac{y}{\nu}\sqrt{\tau_w/\rho}$, $y^*=\frac{y}{\nu}u_\varepsilon$, $u^+=\frac{u}{\sqrt{\tau_w/\rho}}$, $\tau_w=\mu\frac{dU}{dy}$, $u_\varepsilon=(\nu\varepsilon)^{0.25}$		

[a] The Wilcox model equation was converted to an equation for ε.
[b] $\sigma_k=1.4-1.1\exp\left(-\frac{y_\lambda}{10}\right)$.
[c] $\sigma_\varepsilon=1.3-1.0\exp\left(-\frac{y_\lambda}{10}\right)$, where $y_\lambda=y/\sqrt{\frac{\nu k}{\varepsilon}}$.

flow laminarising regime where turbulence is reduced due to the influence of buoyancy and (b) a recovery regime where the flow has past the stage at which it is completely laminarised and new turbulence is generated in the core of the flow due to the greatly distorted velocity profile as a result of a very strong influence of buoyancy. Consider the three DNS results shown in Fig. 3. It can be seen that Case (a) represents a flow in the 'laminarizing' regime, where the Nusselt number ratio is reducing with increase of buoyancy parameter. Case (c) represents a flow in the 'recovery' regime, where the Nu ratio starts to increase with increasing buoyancy parameter due to new turbulence

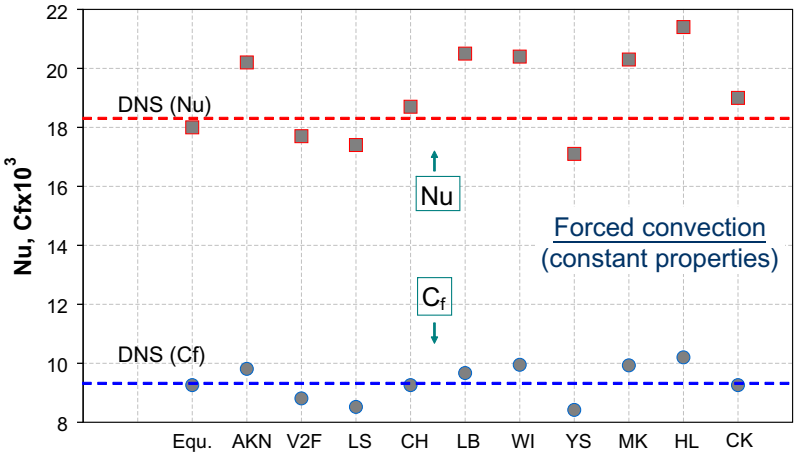

Fig. 2. Values of predicted Nusselt number and friction coefficient from the turbulence models compared with DNS results for conditions of fully developed forced convection.

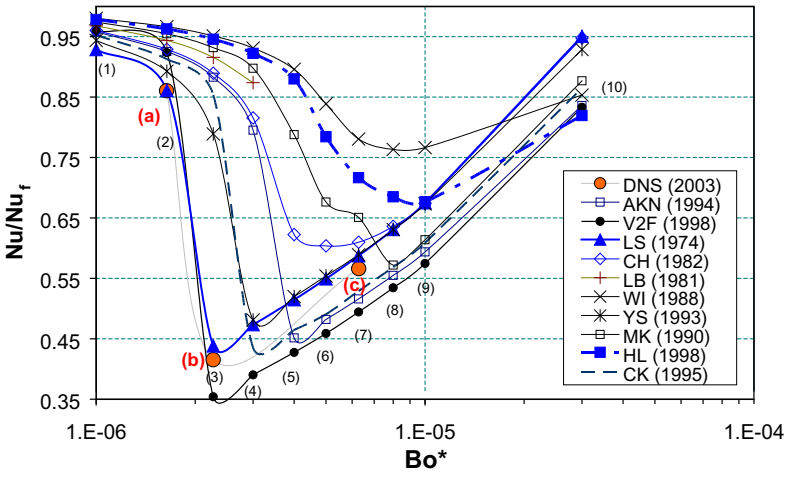

Fig. 3. Influences of buoyancy on heat transfer from simulations made using the turbulence models and in the DNS calculations.

generation. When the buoyancy influence is extremely strong, the Nu ratio may even be higher than unity, but no such cases have been considered in this study. It can also be seen from the figure that the maximum heat transfer impairment occurs in DNS Case (b) and as will be shown later, this case represents an extreme situation where the flow is close to being completely laminarised.

The performance of the various models can now be assessed by comparing their predictions with the DNS data. It is clear from Fig. 3 that to some extent all turbulence models are able to reproduce the general trend of the effects of buoyancy on heat transfer exhibited by the DNS data involving an initial impairment followed by recovery. However, the detailed comparison with the DNS behaviour varies significantly. The success or otherwise of a model can be judged on two counts, i.e., the extent of the maximum impairment of heat transfer predicted and the value of buoyancy parameter at which this occurs. It is clear that the LS model out-performs all other models with a very close reproduction of the Nusselt number ratio for each of the three cases. This model has also been found to perform well in a number of previous studies of mixed convection based on comparisons with experimental data, although some defects have been identified under certain flow conditions [15]. These include laminarization sometimes being predicted too early and the recovery being largely delayed. Nevertheless, it is interesting to note that although many newer models have been developed, often based on information available from DNS studies, few of them perform as well as the LS model does. In fact, recently Cotton and Kirwin [26] made a specific effort to improve the performance of the LS model for conditions of mixed convection but concluded that little was able to be achieved. In the present tests, this revised LS model (CK) clearly performs well for conditions of forced convection (see Fig. 2) but is slightly less effective than the original LS model in reproducing the buoyancy effect. Other k–ε models which perform reasonably well are the YS and AKN models. On the other hand, the CH model exhibits a significant delay in achieving maximum impairment and also under-predicts the extent of it. The results from two newer models, MK and HL are even worse. As

far as the non k–ε models are concerned, the V2F appears to do very well with only a slight over-prediction of the maximum impairment, whereas the Wilcox's k–ω model prediction is the worst of all.

It appears that the models tested can be put into two groups: namely, Group 1, consisting of LS, CK, AKN, YS and V2F, which can predict the buoyancy-induced impairment of heat transfer reasonably well and Group 2, consisting of CH, MK, HL and WI, which is unable to do so. Detailed comparison of the velocity and turbulence predictions with DNS data has shown that the results from Group 1 largely show similar characteristics and so the results from Group 2. In this paper, further comparison with DNS data will be mainly made for two representative models only, i.e., the LS model, representing Group 1 which perform reasonably well, and the HL model, representing Group 2 which perform relatively poorly.

4.1.2. Friction coefficient

As in the case of heat transfer, there are again two competing effects acting on the friction in a buoyancy-aided flow, namely, the direct effect of modification of the mean flow field which causes friction to tend to increase and reduction in turbulent mixing which tends to cause the friction to reduce. The friction coefficient in any particular flow may be increased or decreased dependent on the relative contributions of the two effects. Fig. 4 shows friction coefficient normalized using the corresponding forced convection value for the same cases shown in Fig. 3. It can be seen from the DNS data that with increasing influence of buoyancy, the normalized friction coefficient initially decreases, taking a value lower than unity. However, as the buoyancy is further increased, the trend reverses and the friction coefficient increases. The difference between the behaviour of Nusselt number ratio and friction coefficient ratio is clearly apparent. The reduction of the friction coefficient due to laminarisation is significantly less than that of heat transfer. Friction coefficient ratio actually rises to a value greater than unity in Case (c) although Nusselt number ratio for that case is still much less than one. It is apparent that in buoyancy-influenced flow the relationship between momentum transfer and heat transfer is less direct than in forced convection.

The performance of the various models in predicting the effect of buoyancy on friction can be seen from Fig. 4. The friction coefficient ratio predicted by the AKN, V2F, LS, and CK models show some initial reduction with the increase of buoyancy influence, but the extent of the reduction predicted by all of the models except for V2F is far less than that exhibited in the DNS results. Other models completely fail to predict the reduction, instead, showing a systematic increase of friction with the increase of buoyancy influence.

It is of interest to note the different trends of friction coefficient and Nusselt number ratios exhibited by the various models. A good description of one parameter does not always coincide with a good description of the other. For example, the Nusselt number ratio is very closely reproduced by the LS model for all the cases but the friction coefficient behaviour is not well reproduced in two of the cases. With the AKN model, the Nusselt number ratio in Case (c) is significantly under-predicted but the friction coefficient ratio is closely reproduced.

4.2. The mean flow and turbulence fields

Figs. 5 and 6 show the profiles of normalized mean velocity, turbulent kinetic energy, and turbulent shear stress for the various test cases using the LS and HL models, respectively. Also shown in the figures for direct comparison are the corresponding results from the DNS simulations.

It is useful to summarize the characteristics exhibited by the DNS data first. For Case (a), the velocity profile (Fig. 5a) is very similar to that for forced convection and the turbulence quantities (k and uv, Fig. 5b and c) are only slightly reduced. For Case (b), the velocity profile is very much flattened in the core (in fact showing a slightly

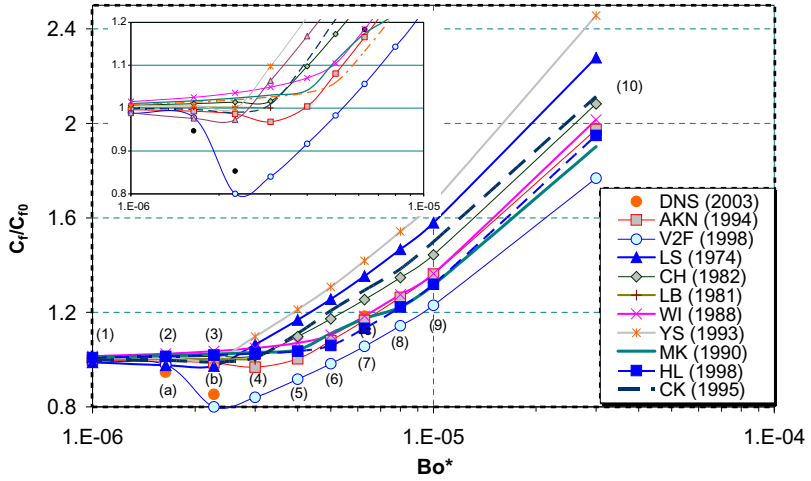

Fig. 4. Influences of buoyancy on friction from simulations made using the turbulence models and in the DNS calculations.

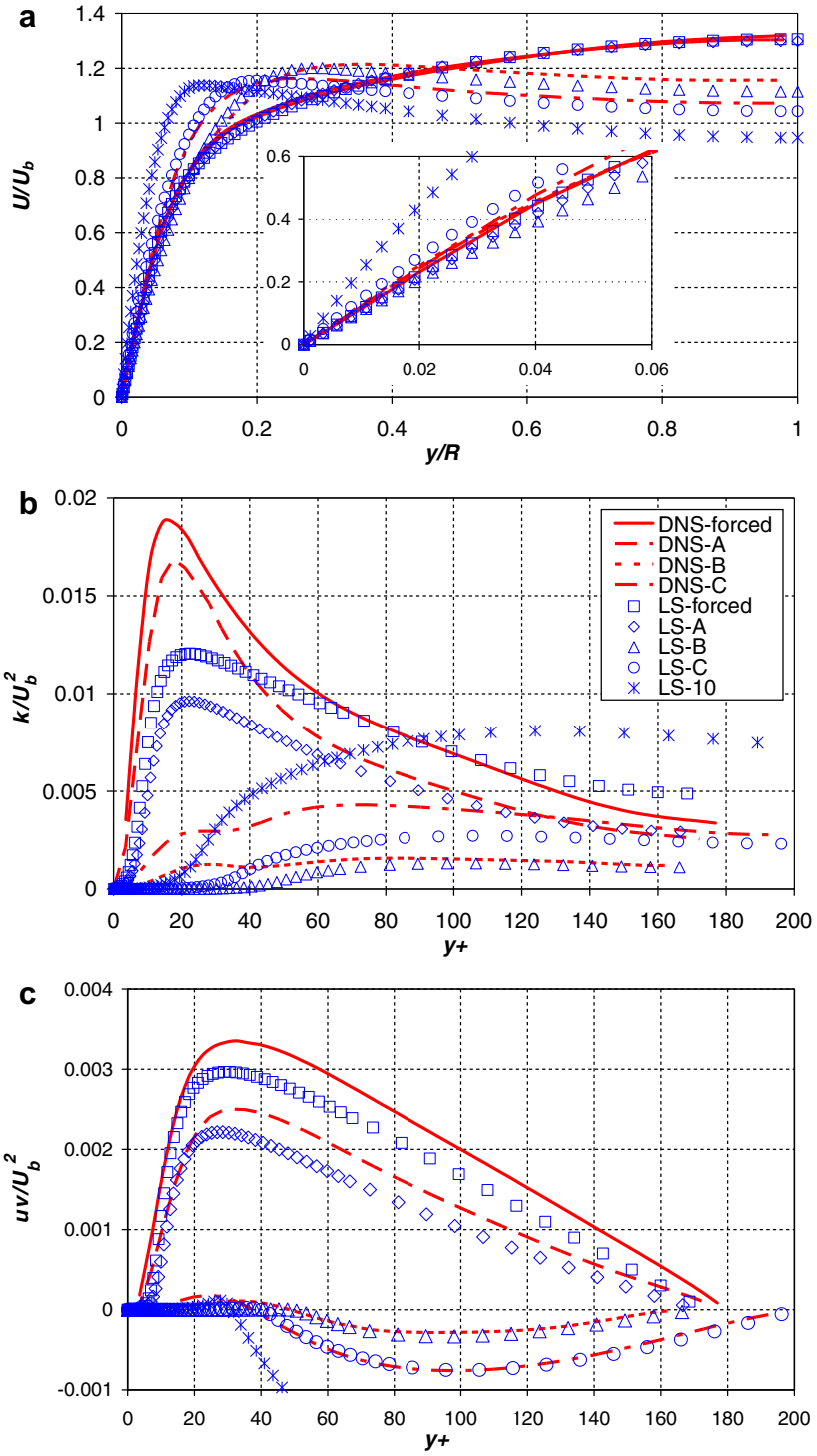

Fig. 5. Mean velocity and turbulent quantities predicted using the LS model: (a) velocity, (b) turbulent kinetic energy and (c) turbulent shear stress.

inverted shape) and the turbulence quantities are reduced to a very low level. The turbulent shear stress uv is slightly negative in the core which indicates that the flow is about to enter the recovery regime. With further increase of buoyancy (Case (c)), the velocity profile is more severely inverted and more turbulence is being produced.

As can be seen from Fig. 5, the velocity profiles predicted by the LS model agree extremely well with the DNS data. The distortion of the mean flow due to buoyancy is very well captured. But very close to the wall, the LS prediction does not follow closely the DNS data, which, although not clearly shown in this figure, can be inferred from the friction results shown in Fig. 4. The LS prediction of turbulence kinetic energy in forced convection shows a much reduced peak near the wall in comparison with the DNS. This is a well known defect of the LS model. In spite

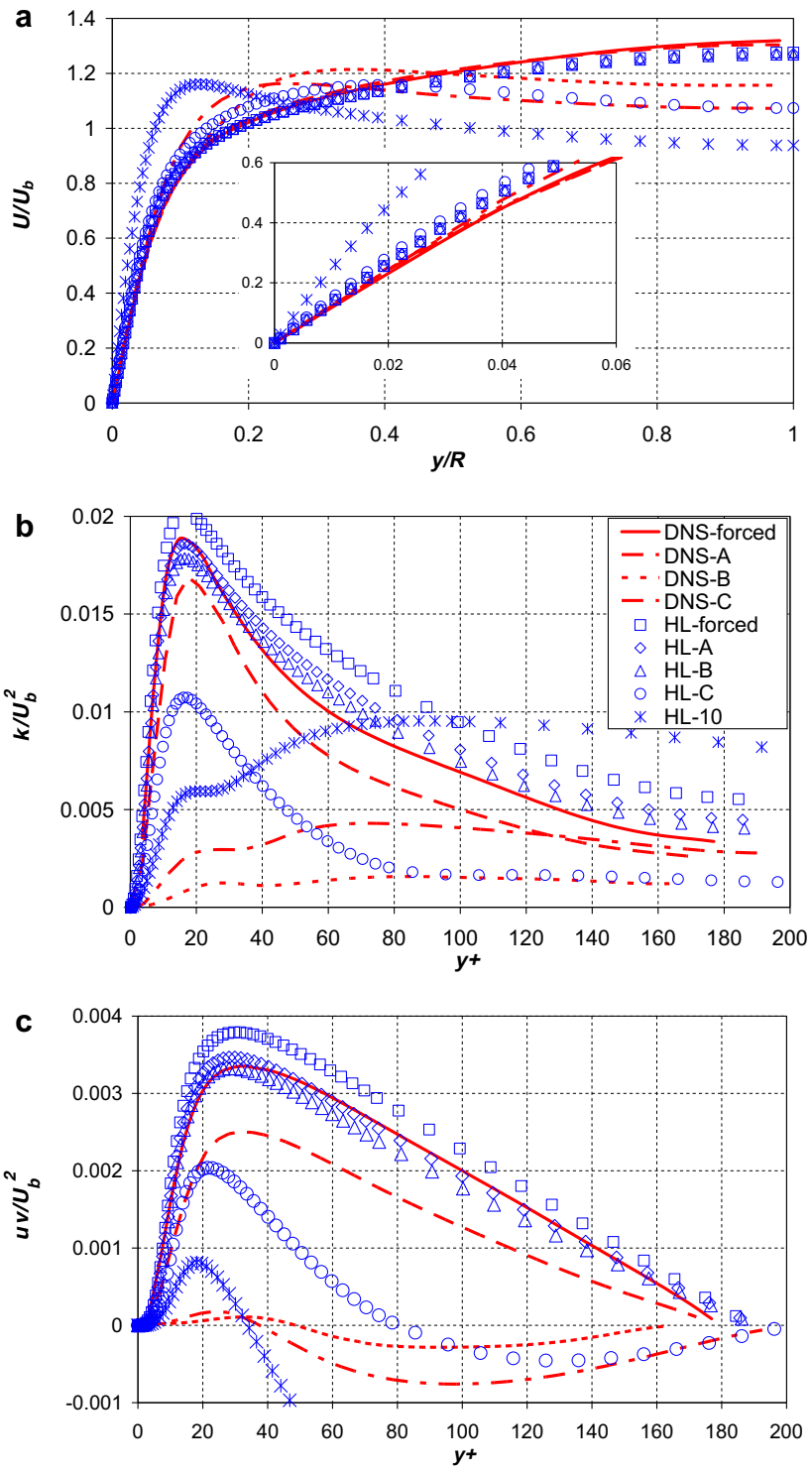

Fig. 6. Mean velocity and turbulent quantities predicted using the HL model: (a) velocity, (b) turbulent kinetic energy and (c) turbulent shear stress.

of this, the effect of the buoyancy on turbulence reduction seems to be very well captured. The recovery of turbulent shear stress in the core in Cases (b) and (c) is extremely well reproduced but the level of turbulent kinetic energy is under-predicted.

There is however a significant difference between turbulence regeneration near the wall predicted by the LS and that of the DNS. The DNS results show that both uv and k increase near the wall (although by only quite small amounts) as well as in the core region in the recovery case (Case c) with increasing buoyancy influence. However, the LS model predicts zero k and uv in the near wall region for this and all the other recovery cases, i.e., 3–9. This is of particular significance since turbulence near the wall is

important in terms of both momentum and heat transfer. This is at least partly responsible for the under-prediction of the heat transfer recovery found in a number of earlier computational studies under conditions of strong buoyancy influence using the LS model. It is interesting to note however that, in the present study, heat transfer in the recovery case is actually very well reproduced by the LS model (refer to Fig. 2). However close inspection of the results reveals that such a match has been achieved as a result of two incorrectly reproduced effects cancelling each other out, i.e., under-predicted turbulent diffusion and an over-predicted advection.

As can be seen from Fig. 6, the HL model also predicts the trends of the turbulence reduction followed by regeneration along with a change in the mean velocity from a flattened to an inverted profile under the influence of increasing buoyancy. However the details are very different from those exhibited by the LS model results (and other Group 1 models). The reduction of turbulence with increasing buoyancy occurs far too slowly in the HL model results leading to big discrepancies with the DNS data. In the series of cases with increasing buoyancy influence, there is none where turbulence is completely suppressed as found in the DNS results and those obtained by Group 1 models. With the HL model, negative turbulence shear stress begins to developing in the core of the pipe in cases where its level in the near wall region is still high (e.g., Case (c) and Case 10). With further increase of buoyancy influence, the turbulent shear stress near the wall reduces and eventually falls to zero. However, this process is accompanied by a continuous increase in the magnitude of the negative turbulent shear stress in the core. In accordance with this trend, turbulent kinetic energy first reduces as the buoyancy influence is increased, but well before a complete laminarization is reached, it starts to increase again. It is also of interest to note that the maximum reduction in Nusselt number does not always coincide with the minimum turbulence in Group 2 predictions. For the HL model, the maximum heat transfer impairment occurs in Cases 8 and 9. However, the turbulent kinetic energy and shear stress continue to reduce in the near wall region with further increase in buoyancy influence (not shown here). This mismatch can be explained by the fact that the contribution of the increasing advection, which enhances heat transfer, outweighs the effect of the reduction in turbulence in these particular cases.

4.3. Understanding the reasons for the diverse performance of the various turbulence models

Following the ideas of Petukhov and Polyakov [33], the influence of buoyancy on turbulence can be viewed as resulting from two distinct mechanisms, namely, the direct effect and the indirect effect. The direct effect refers to turbulent energy production/destruction arising as a result of density fluctuations in a buoyancy-influenced flow. This is accounted for by the buoyancy production terms in the k and ε equations. It has been found in a number of previous studies that this effect is only of secondary importance in the case of buoyancy-influenced flow in vertical tubes. The indirect effect is essentially the response of turbulence to the distortion of the mean flow field resulting from the influence of buoyancy. For turbulent mixed convection in a vertical tube, this is the principal mechanism responsible for the impairment or enhancement of heat transfer. Consequently, the indirect effect will be the main focus of the following section. Predictions of direct buoyant production and its importance relative to the indirect shear production will however be briefly discussed in Section 4.3.3.

4.3.1. The eddy viscosity and damping functions

Under the framework of eddy viscosity turbulence models, the ultimate link between turbulence modelling and the mean flow is through the turbulent viscosity μ_t. Consequently the performance of a turbulence model in predicting the mean flow and thermal fields is reflected by the way in which μ_t is predicted. For most turbulence models, μ_t is modelled as the product of a characteristic velocity $k^{1/2}$ and a characteristic length ($k^{3/2}/\varepsilon$). Thus

$$\mu_t \propto k^2/\varepsilon$$

With a low-Reynolds number turbulence model, along with other considerations, a damping function f_μ is introduced into the above expression to describe the near wall behaviour involving the breakdown of the proportionality between μ_t and k^2/ε, i.e., $\mu_t \propto f_\mu k^2/\varepsilon$. In fact the damping functionf_μ is an important feature of low-Reynolds number modelling which distinguishes one model from another and influences their performance. Now, in order to understand the behaviour of the various models in buoyancy-influenced flows, it is clearly of interest to examine the predictions of the turbulent viscosity under the various flow conditions, and moreover, to understand how this has been arrived at. Thus we should examine the predictions of the f_μ and k^2/ε.

The effect of increasing the influence of buoyancy on the turbulent viscosity can be seen from the DNS results shown in Fig. 7a. The response of the eddy viscosity is markedly different in the near wall region ($y+ < 50$) and in the core. In the wall region the eddy viscosity reduces slightly when the buoyancy influence is weak, such as in Case (a), and becomes effectively zero when laminarization occurs, Case (b). The extent of the region where μ_t is effectively zero reduces as the buoyancy influence is increased further and recovery takes place (Case c). In the core region the eddy viscosity only reduces slightly in the strongly buoyancy-influenced cases.

It can be seen from Fig. 7a that the prediction by the LS model of the buoyancy effect on turbulent viscosity is in excellent agreement with that exhibited in DNS. The extent to which turbulent viscosity is damped out is precisely predicted. In fact, all Group 1 models are able to capture the general trend of the variation of eddy viscosity with the increase of buoyancy influence. In each case, the eddy

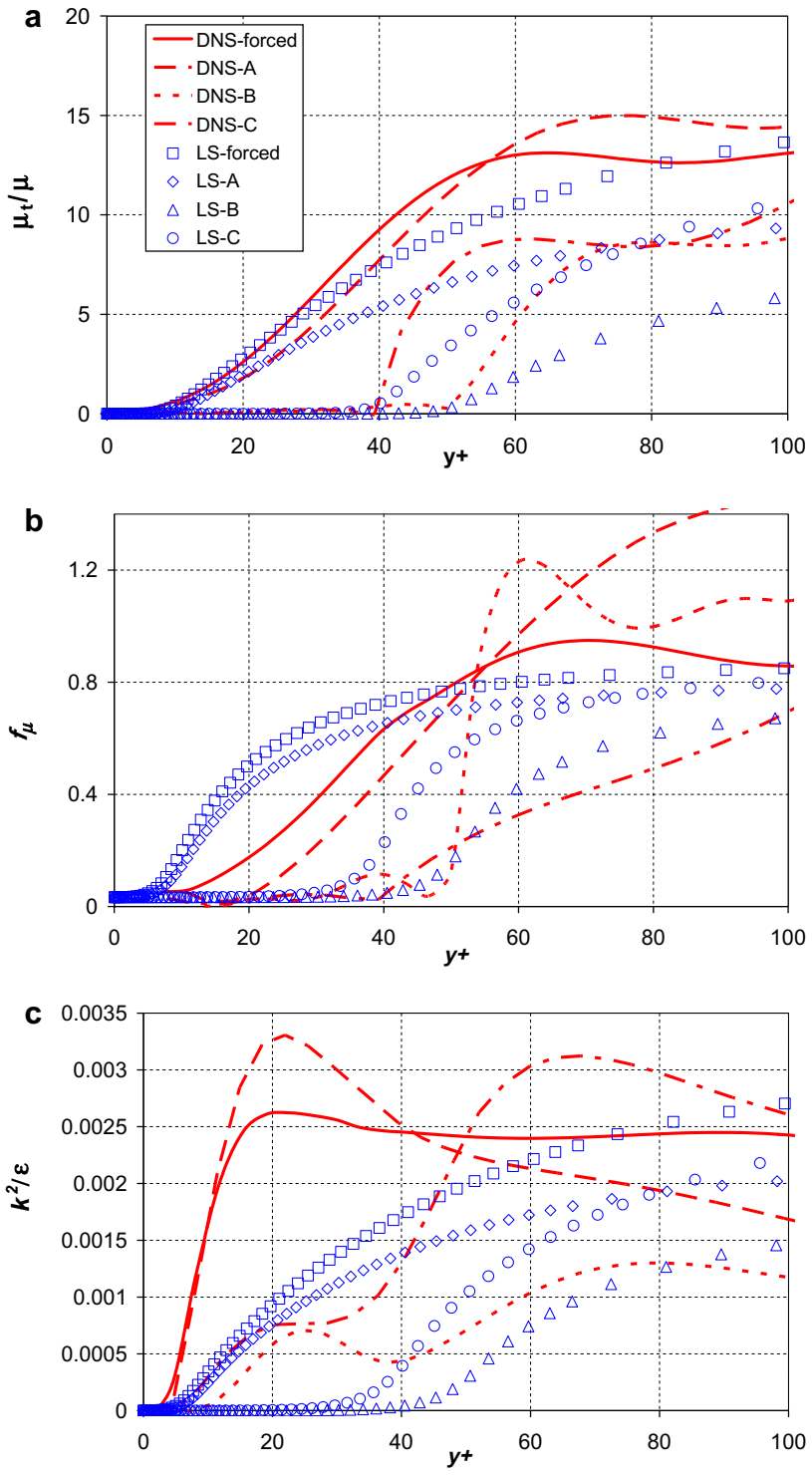

Fig. 7. Eddy viscosity and associated quantities predicted using the LS model: (a) μ_t/μ, (b) f_μ and (c) k^2/ε.

viscosity reduces with increasing buoyancy influence until a complete laminarization occurs (although the buoyancy parameter at which this occurs may be different for each model). With further increase of buoyancy influence, the region of zero eddy viscosity reduces which indicates that some of turbulence recovery is occurring. Clearly the fact that the eddy viscosity is well predicted by the LS model and other Group 1 models is in line with their good performance in the heat transfer results shown in Fig. 3. It should be noted however that there is a small but important difference between the model predictions and the DNS data. The DNS data show a small recovery of μ_t occurring in the near wall region in Case c and this is expected to grow as the buoyancy influence is increased. With the LS model (and

other models), however, the eddy viscosity predicted remains zero in the wall region for all of the 'recovery' cases. For example, the eddy viscosity in Case 10 still remains zero near the wall even though the recovery is well underway.

The poorer performance of Group 2 models, such as CH, HL and MK, in calculating the friction and heat transfer for buoyancy-influenced flows (see Figs. 3 and 4) can also be traced back to the way they reproduce the response of turbulent viscosity to increase of buoyancy influence. Consider the HL model for example (see Fig. 8a). Although the predicted eddy viscosity does reduce with the increase of buoyancy influence, it only does so very slowly. Even in the extreme case where the buoyancy influ-

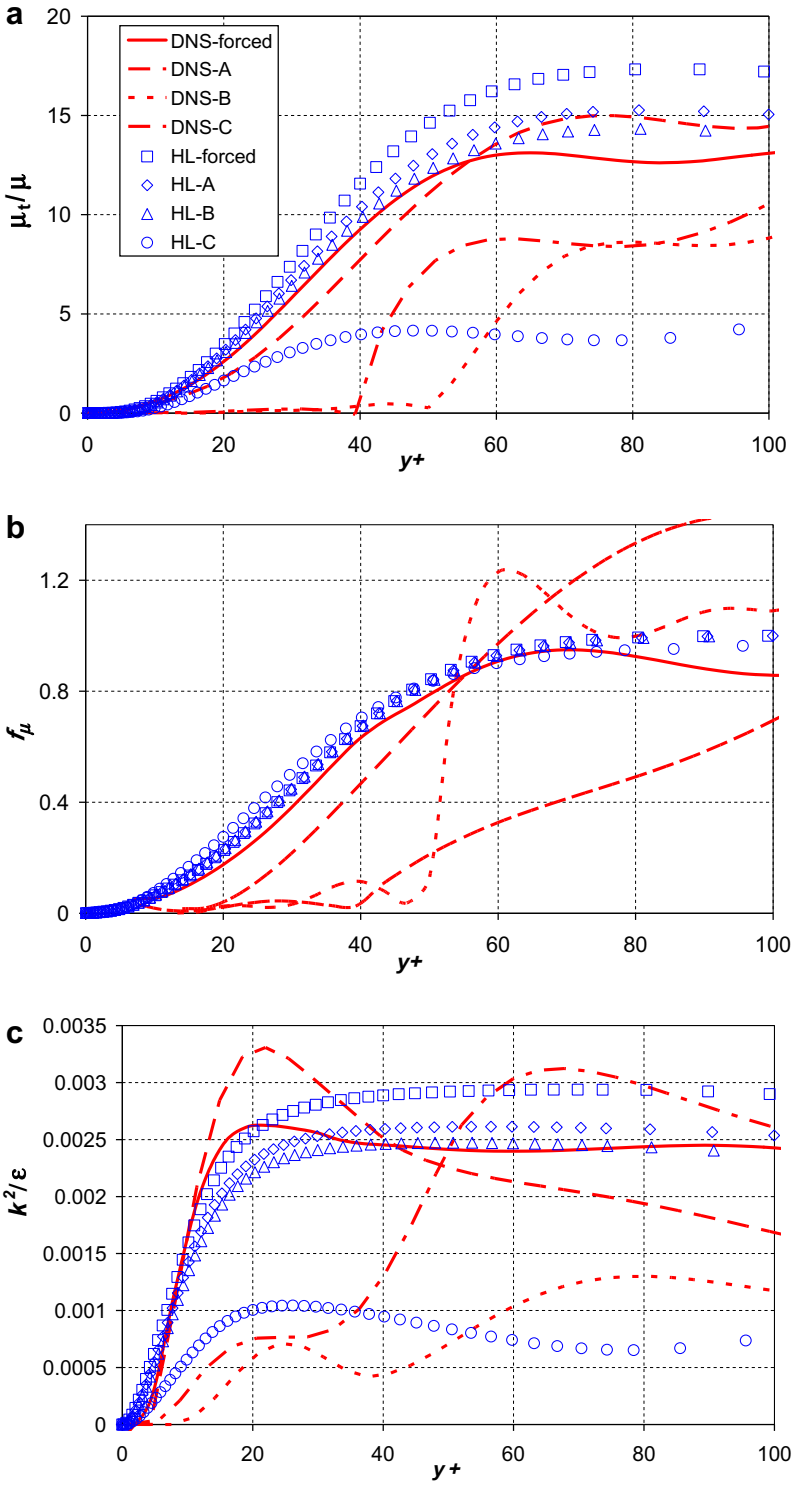

Fig. 8. Eddy viscosity and associated quantities predicted using the HL model: (a) μ_t/μ, (b) f_μ and (c) k^2/ε.

ence is many times that of the critical buoyancy parameter indicated by the DNS, the eddy viscosity is still not completely suppressed. Such a slow reduction of the eddy viscosity with the influence of buoyancy is clearly consistent with under-prediction of the deterioration of heat transfer.

The distributions of the damping function f_μ and the term k^2/ε are examined next. These are presented in Figs. 7b and c and 8b and c for the LS and HL models, respectively. Focusing on the near wall region, it is clear from the DNS data that the damping functionf_μ reduces to almost zero near the wall when the buoyancy influence is strong. The term k^2/ε also reduces but its value is far greater than zero even when the flow is laminarized. It can be seen from Fig. 7b that the LS model is able to reproduce the variations of the damping function f_μ very well. However, the reduction of the term k^2/ε with buoyancy is significantly over predicted, with zero values predicted in the wall region for the recovery cases. It is now clear that it is this part of model, i.e., the prediction of the ratio k^2/ε, rather than f_μ which causes the under-response of the turbulent viscosity in the recovery regime, and is responsible for the under-prediction of k and uv in the wall region. In contrast to the LS model, the HL model appears to completely fail to predict the response of f_μ to buoyancy influence, giving slightly increased values as buoyancy is increased. This is likely to be the principal reason for the lack of response of turbulence to buoyancy influence in the case of the HL model and other models of that kind, although the

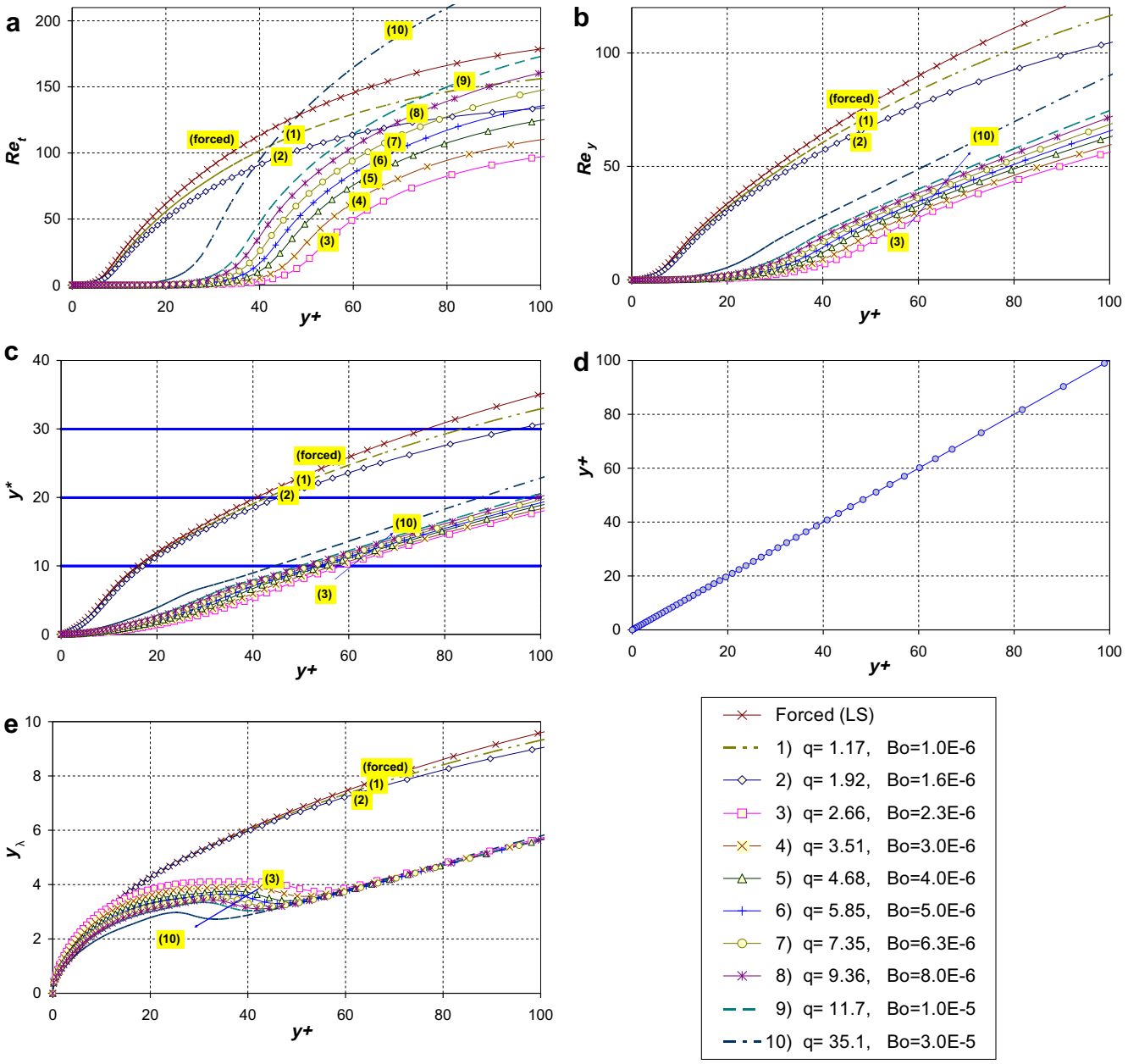

Fig. 9. Controlling parameters used in the damping functions for buoyancy-influenced flows: (a) Re_t, (b) Re_y, (c) y^*, (d) $y+$ and (e) y_λ.

reduction of the term k^2/ε with increasing buoyancy influence is also significantly slower than that exhibited by the DNS data, which also adds to the poor performance of the models.

4.3.2. Selection of parameters used in the damping functions

From the results discussed so far, it is clear that in order for a turbulence model to reproduce the effect of buoyancy on the flow and turbulence, it should have a damping function which responds correctly to buoyancy influence. It is obvious that a pre-requisition for this is that the controlling variable(s) used in the damping functions should respond to the flow variations in an appropriate manner.

Fig. 9 shows the radial distribution of the controlling variables in the damping functions used in the various turbulence models considered in this study. These were calculated using the data from the LS model simulations. Focusing on the near wall behaviour, it can be seen that Re_t, Re_y and y^* are able to respond to the changes of flow condition. The values of these parameters reduce significantly as the flow is laminarized. The turbulent Reynolds number Re_t, which has the feature of not involving distance from the wall, appears to show the most distinct response. On the other end of the spectrum, the parameter y_λ exhibits very little response to the change of flow conditions in the wall region. Therefore this parameter along with y^+ (which by definition does not change with flow conditions) is clearly not suitable for capturing the 'non-equilibrium' effects exhibited in flows such as the buoyancy-influenced ones considered here.

The ideas discussed above are consistent with the performance exhibited by the various turbulence models. In particular, the damping functions f_μ of the HL and CH models are based on y_λ and y^+ respectively and the performance of these models is poor. The damping function of the LS model is based on Re_t and this is clearly one of the features which enable that model to perform well. It is interesting to note that most of the other models tested here use a combination of Re_t and one other parameter in the formulation of their damping functions and that the performance of those models can be ranked between the LS model and the CH model. It is obvious that the fine detail of the formulation of the damping function is also of crucial importance in determining the response of the model to

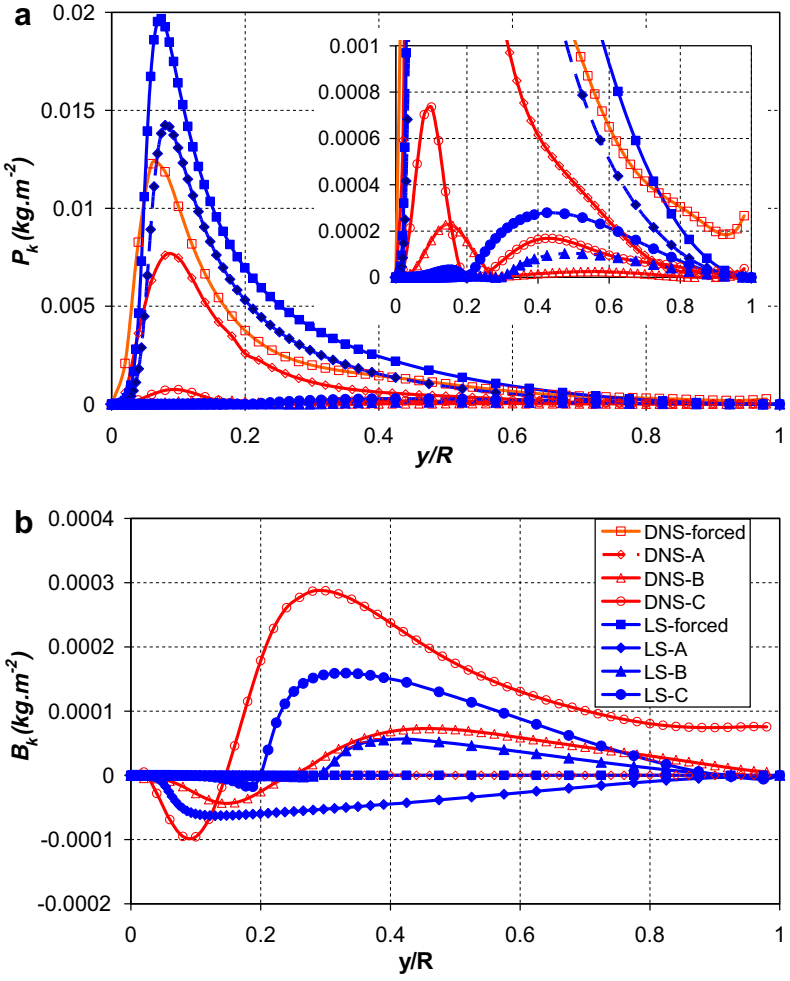

Fig. 10. Production of turbulent kinetic energy predicted using the LS model: (a) shear production and (b) buoyancy production.

non-equilibrium conditions. A good illustration of this is the contrast between the performance of the LS model and that of the model due to Jones and Launder (JL) [34]. Although the two models use the same variable Re_t, and only slightly different formulations of the damping function, their performances have been found to be very different [15].

4.3.3. Production of turbulent kinetic energy

Figs. 10 and 11 show the predicted production of turbulent kinetic energy through the action of shear and buoyancy using the LS and HL models, respectively. Also shown in the figures are results extracted from the DNS calculations. It is clear from the latter that the effect of direct buoyancy production is negligible in the laminarizing regime (Case a). In the fully laminarized and recovery conditions (Cases b and c), the direct buoyancy production increases near the wall but is yet still significantly lower than the shear production (about 15%) and acts in opposition to it. In the core, however, the buoyancy production is roughly the same as the shear production and has the same sign. It can be seen from Fig. 10 that the shear production near the wall is significantly under-predicted by the LS model. This is consistent with the under-prediction of turbulent quantities (uv and k) in this region which was discussed earlier and is clearly an important issue that needs to be addressed when improvement of the performance of such turbulence models is sought. Both the shear production and the buoyancy production in the core are closely reproduced. On the other hand, the shear production predicted by the HL model responds very slowly to the influence of buoyancy near the wall, which explains the results discussed earlier concerning the slow suppression of turbulence as a result of buoyancy influence.

4.3.4. Turbulent Prandtl number

Turbulent heat flux $\overline{u_i't'}$ can be related to temperature gradient by the expression $\overline{u_i't'} = \alpha_t \frac{\partial \phi}{\partial x_i}$, in which α_t is the so-called turbulent diffusivity of heat. Arguments based on the idea of an analogy between heat and momentum transport suggest that α_t might be closely related to ν_t. For convenience, turbulent Prandtl number has been used which is defined based on the ratio of the two, i.e., $Pr_t = \frac{\nu_t}{\alpha_t}$. It is frequently argued on the basis of experimental evidence that this parameter varies very little within a flow and also from flow to flow and it is frequently assigned a constant value of 0.9 in order to model turbulent heat

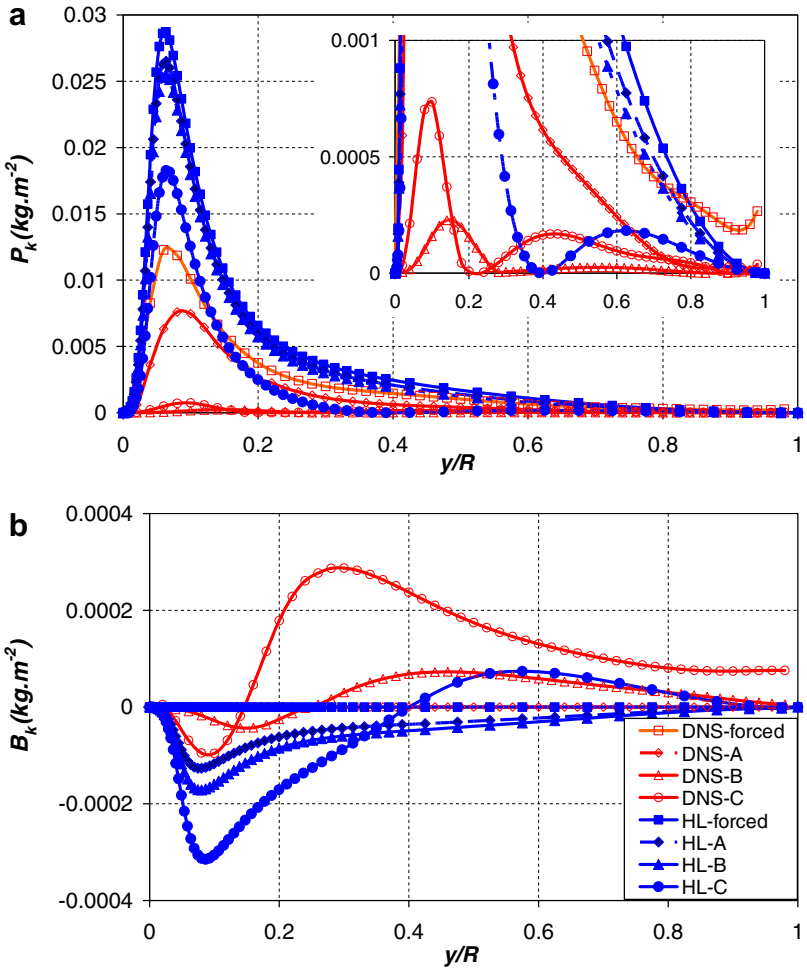

Fig. 11. Production of turbulent kinetic energy predicted using the HL model: (a) shear production and (b) buoyancy production.

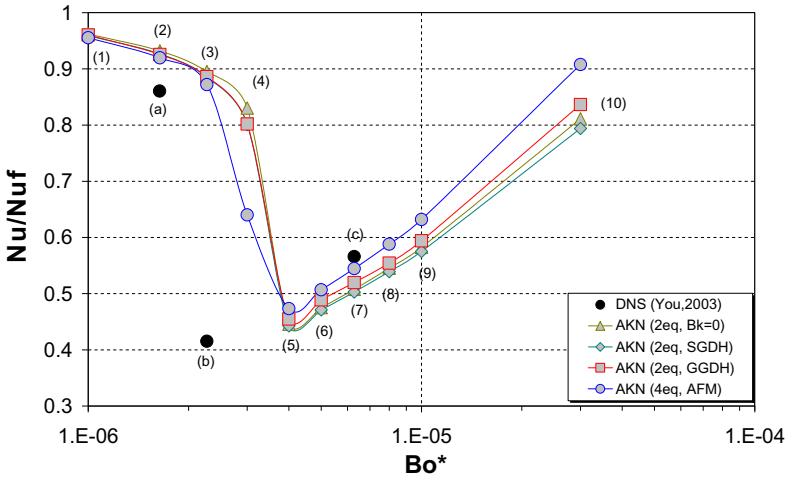

Fig. 12. Effect of using alternative models for buoyancy production of turbulence.

transfer. However it might be expected that such an analogy is likely to be followed less closely in non-equilibrium flows such as buoyancy-influenced ones considered here and therefore, that for such conditions if a turbulent Prandtl number Pr_t is used, it should be vary with flow condition. In order to avoid having to use a constant Pr_t, a number of turbulent heat transfer models have been proposed involving transport equations for temperature variance $\overline{t^2}$ and its dissipation rate ε_t. In this study we have conducted several simulations using such a heat transfer model proposed by Abe et al. [35], referred to as Eq. (3) AKN model. In addition to allowing for a variable Pr_t, the availability of $\overline{t^2}$ and ε_t has also been used to improve the formulation of the turbulence buoyancy production terms. Here, we have abandoned the GGDH approach in preference to a more advanced algebraic flux model (AFM) due to Kenjeres et al. [36] (see Appendix).

Fig. 12 shows the comparison of the Nusselt number ratios obtained from simulations using the two-equation and Eq. (3) AKN turbulence models. It can be seen from the figure that the results from Eq. (3) model consistently show some improvements over the two-equation model results. In particular, the onset of impairment occurs earlier and so does the recovery of heat transfer. However, the improvement is relatively small and the performance is still not as good as that of the LS model. In order to investigate the significance of the buoyancy production further, we have also conducted simulations with this term modelled using the simple gradient diffusion hypothesis (SGDH) in one series of calculations, see Appendix for formulation, and with the buoyancy production term set to zero in another. The results are also shown in Fig. 12. It is clear that the differences between the results obtained from the GGDH, SGDH and zero-buoyancy production simulations are insignificantly small, confirming our view that the buoyancy production of turbulence does not play a significant role and that the indirect effect of buoyancy on turbulence dominates in the case of mixed convection in vertical channels.

5. Conclusions

RANS simulations of turbulent mixed convection in a vertical tube have been conducted for an idealized condition, in which the effects of non-uniformity of fluid properties, other than those which cause an influence of buoyancy, have been removed. A number of low-Reynolds number, two and four-equation, turbulence models of eddy viscosity type have been used. In each case, the results of the simulations have been compared with DNS data for the same conditions. This has enabled an assessment to be made of the ability of the models to reproduce the effects of buoyancy on both turbulence and heat transfer. More importantly, a better understanding of the underlying reasons for the diverse performance of the various turbulence models has been arrived at. This has shed some light on how the ability of such models to predict buoyancy-influenced, turbulent flow and heat transfer might be improved.

The present study has shown that the indirect influence of buoyancy on turbulence in a heated vertical tube is the dominant mechanism which causes laminarization and deterioration of heat transfer. Under such conditions, the influence of buoyancy on direct production of turbulence has proved to have a negligible effect. However, it does have a noticeable effect, but still only secondary one, as the influence of buoyancy is increased to the stage where turbulence production recovers and the effectiveness of heat transfer improves. This explains why the use of some recently developed models which have been specifically aimed at the simulation of buoyancy-driven cavity flows and buoyancy-influenced horizontal flows does not lead to as big an improvement in the prediction of turbulent mixed convection in vertical pipes as might have been expected. In such models attention has mostly been focussed on the description of the direct contribution of buoyancy, which is known to be important in buoyancy-driven cavity flows and horizontal flows but is not so important in turbulent mixed convection in vertical pipes.

Rather surprisingly, the models which reproduce the general trends of the effects of buoyancy influence in vertical turbulent mixed convection most closely are some rather early ones such as the LS and YS models. However, it has become clear that although these models predict eddy viscosity reasonably well, this is only achieved as a result of the effects of inaccurate representations of its two components, k^2/ε andf_μ, cancelling out. The reduction of the term k^2/ε due to the influence of buoyancy is significantly overpredicted by these models. This behaviour is partly responsible for them being unable to reliably reproduce the recovery of turbulence and enhancement of heat transfer which is known to occur under conditions of strong mixed convection in vertical tubes. In future model development, an important challenge with such flows will be to produce sufficient recovery of turbulence, in particular achieving the high values of k^2/ε near the wall seen in the DNS studies.

Clearly, the performance of a low-Reynolds number turbulence model is very sensitive to the fine detail of the formulation of the damping function and the choice of controlling parameters used is a key factor in enabling it to respond to the 'non-equilibrium' features present. The parameters which exhibit the most satisfactory effects in this respect are Re_t, Re_y, and y^*, whereas parameters such as y^+ and y_λ either do not respond adequately or respond in an undesirable way. Combining more than one variable in the formulation will clearly increase the potential of a model to be successful under a broader range of conditions.

Acknowledgements

The authors gratefully acknowledge the funding for this project provided by UK Engineering and Physical Sciences Research Council (EPSRC) through Grant GR/S19424/02.

Appendix. Modelling of buoyancy production term of turbulent kinetic energy (G_k)

The production of turbulent kinetic energy due to buoyancy is expressed as

$$\rho G_k = g_i\overline{\rho' u_i'} \tag{A.1}$$

Assuming the fluctuation of density is mainly resulted from temperature fluctuation, then

$$\rho G_k = -\beta\rho g_i\overline{u_i\theta}, \quad \text{where} \quad \left(\beta = -\frac{1}{\rho}\frac{\partial\rho}{\partial\theta}\right) \tag{A.2}$$

A.1. Simple gradient diffusion hypothesis (SGDH)

Relating turbulent heat flux to the mean temperature gradient by

$$\overline{u_i\theta} = -\frac{\nu_t}{Pr_t}\frac{\partial T}{\partial x_i} \tag{A.3}$$

we obtain

$$\rho G_k = \beta\rho g_x\frac{\nu_t}{Pr_t}\frac{\partial T}{\partial x} \tag{A.4}$$

where $g_x = -g$ for upward flow, $g_x = g$ for downward flow and $Pr_t = 0.9$.

A.2. Generalised gradient diffusion hypothesis (GGDH)

Following Ince and Launder [36]

$$\overline{u_i\theta} = -c_\theta\frac{k}{\varepsilon}\overline{u_iu_j}\frac{\partial T}{\partial x_j} \tag{A.5}$$

Therefore, $\rho G_k = -\beta\rho g_i\overline{u_i\theta} = c_\theta\beta\rho g_i\frac{k}{\varepsilon}\overline{u_iu_j}\frac{\partial T}{\partial x_j}$, where $c_\theta = 0.3$

Thus,

$$\rho G_k = -c_\theta\beta\rho g_x \times\frac{k}{\varepsilon}\left[\mu_t\left(\frac{\partial U}{\partial r}+\frac{\partial V}{\partial x}\right)\frac{\partial T}{\partial r}+\left(2\mu_t\frac{\partial U}{\partial x}-\frac{2}{3}\rho k\right)\frac{\partial T}{\partial x}\right] \tag{A.6}$$

where $g_x = -g$ for upward flowand $g_x = g$ for downward flow.

A.3. Algebraic flux model (AFM)

Following Kenjeres et al. [37]

$$\overline{u_i\theta} = -C_{\theta1}\frac{k}{\varepsilon}\left(\zeta\overline{u_iu_j}\frac{\partial T}{\partial x_j}+\xi\overline{\theta u_j}\frac{\partial U_i}{\partial x_j}+\eta\beta g_i\overline{\theta^2}\right) + C_{\theta2}a_{ij}\overline{\theta u_j} \tag{A.7}$$

where

$$C_{\theta1} = 0.15, \quad C_{\theta2} = 1.5, \quad \zeta = \xi = \eta = 0.6,$$

$$a_{ij} = \frac{\overline{u_iu_j}}{k}-\frac{2}{3}\delta_{ij} \quad \text{(stress-anisotropy tensor)},$$

$$\overline{u_iu_j} = -\nu_t\left(\frac{\partial U_i}{\partial x_j}+\frac{\partial U_j}{\partial x_i}\right)+\frac{2}{3}k\delta_{ij} \quad \text{(eddy viscosity)}$$

Therefore,

$$\rho G_k = -\rho\beta g_i\overline{u_i\theta} = C_{\theta1}\rho\beta g_i\frac{k}{\varepsilon}\left(\zeta\overline{u_iu_j}\frac{\partial T}{\partial x_j}+\xi\overline{\theta u_j}\frac{\partial U_i}{\partial x_j}+\eta\beta g_i\overline{\theta^2}\right) - C_{\theta2}\rho\beta g_ia_{ij}\overline{\theta u_j} \tag{A.8}$$

Consider $i = x$, i.e., the buoyancy aligns with the main flow,

$$\rho G_k = C_{\theta1}\rho\beta g_x\frac{k}{\varepsilon}\left(\zeta\overline{uv}\frac{\partial T}{\partial r}+\xi\overline{\theta v}\frac{\partial U}{\partial r}+\eta\beta g_x\overline{\theta^2}\right) - C_{\theta2}\rho\beta g_xa_{xr}\overline{\theta v} \tag{A.9}$$

where,

$g_x = -g$ for upward flow, $g_x = g$ for downward flow

$$\overline{\theta v} = -c_\theta\frac{k}{\varepsilon}\overline{v^2}\frac{\partial T}{\partial r} = -c_\theta f_\mu\frac{k^2}{\varepsilon}\frac{\partial T}{\partial r},$$

$$\overline{uv} = -\nu_t\left(\frac{\partial U}{\partial r}+\frac{\partial V}{\partial x}\right), \quad a_{xr} = \frac{\overline{uv}}{k}$$

References

[1] J.D. Jackson, W.B. Hall, Forced convection heat transfer to fluids at supercritical pressure, Turbulence Forced Convection in Channels & Bundles, vol. 2, Hemisphere, New York, 1979, pp. 563–611.

[2] J.D. Jackson, M.A. Cotton, B.P. Axcell, Studies of mixed convection in vertical tubes, Int. J. Heat Fluid Flow 10 (1989) 2–15.

[3] J.D. Jackson, Studies of buoyancy-influenced turbulent flow and heat transfer in vertical passages, in: Keynote Lecture at the International Heat Transfer Conference, IHTC13, Sidney, Australia, 13–18 August, 2006.

[4] J.E. Byrne, E.U. Ejiogu, Combined free and forced convection heat transfer in a vertical pipe, in: Int. Mech. E., Symposium on Heat and Mass Transfer by Combined Forced and Natural Convection, Manchester, UK, 1971.

[5] A.A. Steiner, On the reverse transition of turbulent flow under the action of buoyancy forces, J. Fluid Mech. 47 (1971) 71–75.

[6] A.D. Carr, M.A. Connor, H.O. Buhr, Velocity, temperature and turbulence measurements in air pipe flow with combined free and forced convection, Trans. ASME J. Heat Transfer 95 (1973) 445–452.

[7] A.F. Polyakov, S.A. Shindin, Development of heat transfer along vertical tubes in the presence of mixed air convection, Int. J. Heat Mass Transfer 31 (1988) 987–992.

[8] J.V. Vilemas, P.S. Poskas, V.E. Kaupas, Local heat transfer in a vertical gas-cooled tube with turbulent mixed convection and different heat fluxes, Int. J. Heat Mass Transfer 35 (1992) 2421–2428.

[9] J. Li, J.D. Jackson, Buoyancy-influenced variable property turbulent heat transfer to air flowing in a uniformly heated vertical tube, in: 2nd EF Conference in Turbulent Heat Transfer, Manchester, UK, 1998.

[10] H. Tanaka, A. Tsuge, M. Hirata, N. Nishiwaki, Effects of buoyancy and of acceleration owing to thermal expansion on turbulent forced convection in vertical tubes criteria of the effects, velocity and temperature profiles and reverse transition from turbulent to laminar flow, Int. J. Heat Mass Transfer 16 (1973) 1267–1288.

[11] P.L. Walklate, A comparative study of theoretical models of turbulence for the numerical prediction of boundary layer flows, Ph.D. Thesis, UMIST, 1976.

[12] M.A. Cotton, Theoretical studies of mixed convection in vertical tubes, Ph.D. Thesis, The University of Manchester, 1987.

[13] B.E. Launder, B.L. Sharma, Application of the energy-dissipation of turbulence to calculation of low near a spinning disc, Lett. Heat Mass Transfer 1 (1974) 131–138.

[14] M.A. Cotton, J.D. Jackson, Vertical tube air flows in the turbulent mixed convection regime calculated using a low-Reynolds number k–ε model, Int. J. Heat Mass Transfer 33 (1990) 275–286.

[15] D.P. Mikielewicz, Comparative studies of turbulence models under conditions of mixed convection with variable properties in heated vertical tubes, Ph.D. Thesis, The University of Manchester, 1994.

[16] K.Y. Chien, Predictions of channel and boundary-layer flows with a low-Reynolds number turbulence model, AIAA J. 20 (1982) 33–38.

[17] A. Behzadmehr, N. Galanis, A. Laneville, Low Reynolds number mixed convection in vertical tubes with uniform wall heat flux, Int. J. Heat Mass Transfer 46 (2003) 4823–4833.

[18] N. Kasagi, M. Nishimura, Direct numerical simulation of combined forced and natural turbulent convection in a vertical plane channel, Int. J. Heat Fluid Flow 18 (1997) 88–99.

[19] J. You, J.Y. Yoo, H. Choi, Direct numerical simulation of heated vertical air flows in fully developed turbulent mixed convection, Int. J. Heat Mass Transfer 46 (2003) 1613–1627.

[20] J.H. Bae, J.Y. Yoo, H. Choi, Direct numerical simulations of turbulent supercritical flows with heat transfer, Phys. Fluids 17 (2005) 105104.

[21] C.K.G. Lam, K. Bremhorst, A modified form of the k–ε model for predicting wall turbulence, Trans. ASME 103 (1981) 456–460.

[22] D.C. Wilcox, Reassessment of the scale determining equation for advanced turbulence models, AIAA J. 26 (1988) 1299–1310.

[23] H.K. Myoung, N. Kasagi, A new approach to the improvement of k–ε turbulence model for wall bounded shear flows, JSME Int. J. 33 (1990) 63–72.

[24] Z. Yang, T.H. Shih, New time scale based k–ε model for near-wall turbulence, AIAA J. 31 (1993) 1191–1198.

[25] K. Abe, T. Kondoh, Y. Nagano, A new turbulence model for predicting fluid flow and heat transfer in separating and reattaching flow, Int. J. Heat Mass Transfer 37 (1994) 139–151.

[26] M.A. Cotton, P.J. Kirwin, A variant of the low-Reynolds-number two-equation turbulence model applied to variable property mixed convection flows, Int. J. Heat Fluid Flow 16 (1995) 486–492.

[27] C.B. Hwang, C.A. Lin, Low-Reynolds number modelling of transpired flows, in: 2nd EF Conference in Turbulent Heat Transfer, Manchester, UK, 1998.

[28] M. Behnia, S. Parneix, P.A. Durbin, Prediction of heat transfer in an axisymmetric turbulent jet impinging on a flat plate, Int. J. Heat Mass Transfer 41 (1998) 1845–1855.

[29] R.E. Spall, A.H. Richards, D.M. McEligot, Numerical modelling of strongly heated internal gas flows, in: ASME Heat Transfer/Fluids Engineering Summer Conference, USA, 2004.

[30] A.H. Richards, R.E. Spall, D.M. McEligot, An assessment of turbulence models for strongly heated internal gas flows, in: International Association of Science and Technology for Development Modelling and Simulation Conference, USA, 2004.

[31] B. Deng, W. Wu, S. Xi, A near-wall two-equation heat transfer model for wall turbulent flows, Int. J. Heat Mass Transfer 44 (2001) 691–698.

[32] B.S. Petukhov, V.A. Kurganov, A.I. Gladuntsov, Turbulent heat transfer in tubes to gases with variable physical properties, Heat Mass Transfer 1 (1972) 117–127.

[33] B.S. Petukhov, A.F. Polyakov, Heat Transfer in Turbulent Mixed Convection, Hemisphere, New York, 1988.

[34] W.P. Jones, B.E. Launder, The prediction of laminarization with a two-equation model of turbulence, Int. J. Heat Mass Transfer 15 (1972) 301–314.

[35] K. Abe, T. Kondoh, Y. Nagano, A new turbulence model for predicting fluid flow and heat transfer in separating and reattaching flows-II. Thermal field calculations, Int. J. Heat Mass Transfer 38 (1995) 1467–1481.

[36] N.Z. Ince, B.E. Launder, Three-dimensional and heat-loss effects on turbulent flow in a nominally two-dimensional cavity, Int. J. Heat Fluid Flow 16 (1995) 171–177.

[37] S. Kenjeres, S.B. Gunarjo, K. Hanjalic, Contribution to elliptic relaxation modelling of turbulent natural and mixed convection, Int. J. Heat Fluid Flow 26 (2005) 569–586.